Biogeosciences Discuss., https://doi.org/10.5194/bg-2018-479
Manuscript under review for journal Biogeosciences
Discussion started: 10 December 2018

Iron minerals inhibit the growth of bacteria via a free-radical mechanism: : Implications for soil carbon storage

Hai-Yan Du[1], Guang-Hui Yu[1, 2], Fu-Sheng Sun[1, 2], Muhammad Usman[3, 4], Bernard A. Goodman[5], Wei Ran[1], Qi-Rong Shen[1]

1. Jiangsu Provincial Key Lab for Organic Solid Waste Utilization, College of Resources & Environmental Sciences, Nanjing Agricultural University, Nanjing 210095, China

2. Institute of Surface-Earth System Science, Tianjin University, Tianjin 300072, China

3. Environmental Mineralogy, Center for Applied Geosciences, University of Tübingen, 72074 Tübingen, Germany

4. Institute of Soil and Environmental Sciences, University of Agriculture, Faisalabad 38040, Pakistan

5. College of Physical Science and Technology, Guangxi University, Nanning 530004, Guangxi, China

Correspondence to: Guang-Hui Yu (yuguanghui@njau.edu.cn or yuguanghui@tju.edu.cn)

Biogeosciences Discuss., https://doi.org/10.5194/bg-2018-479
Manuscript under review for journal Biogeosciences
Discussion started: 10 December 2018

Abstract. Natural minerals in soil can inhibit the growth of bacteria that protect organic carbon from decay. However, the mechanism inhibiting the bacterial growth remains poorly understood. Here, using a series of cultivation experiments and biological, chemical and synchrotron-based spectral analyses, we showed that kaolinite, hematite, goethite and ferrihydrite had a significant inhibitory effect on the growth of *Pseudomonas* J12, which was more prominent with a concentration of 25 mg mL^{-1} than it was with either 10 mg mL^{-1} or 5 mg mL^{-1}. In contrast, montmorillonite promoted the growth of *Pseudomonas* J12. Compared to Al-containing minerals, Fe(III)-containing minerals produced more hydroxyl radical ($HO^{\bullet}$) that have high efficiency for the inhibition of bacteria. Moreover, a significant positive correlation between $HO^{\bullet}$ radical and Fe(II) was found, suggesting that Fe(II) contributes to the generation of $HO^{\bullet}$. Furthermore, both micro X-ray fluorescence and X-ray photoelectron spectroscopies indicated that surface Fe(III) was reduced to Fe(II) which can produce $HO^{\bullet}$ through the well-known Fenton reaction series. Together, these findings indicate that the reduced surface Fe(II) derived from Fe(III)-containing minerals inhibit bacteria via a free-radical mechanism, which may further contribute to soil carbon storage.

Keywords: Fenton reaction; hydroxyl radical ($HO^{\bullet}$); inhibition of bacterial growth; iron minerals; soil carbon storage

Biogeosciences Discuss., https://doi.org/10.5194/bg-2018-479
Manuscript under review for journal Biogeosciences
Discussion started: 10 December 2018

1. Introduction

A variety of minerals exhibit bacterial inhibition properties by releasing Al(III) or Fe(II) (Morrison et al., 2014; McMahon et al., 2016; Williams, 2017). Hence, natural minerals have long been used as bactericidal agents for human pathogens (Williams and Haydel, 2010; Williams et al., 2011). The bacterial inhibition property of a mineral is associated with the particular chemistry and with the mineral properties, resulting in the various bacterial inhibition mechanisms of minerals (Williams et al., 2008). Iron oxides are abundant in terrestrial and aquatic environments and exist predominantly as ferric minerals such as goethite, ferrihydrite, and hematite (Cornell and Schwertmann, 2003; Meunier, 2005; Chesworth, 2008). Due to the ubiquity of soil iron minerals and their distinct inhibition properties, which may affect soil carbon storage and nutrient turnover, investigations of the inhibitory potential of iron minerals on microorganisms are of great importance.

To better understand the inhibition of bacteria by minerals, the mineral type and size should be examined. Previous studies have demonstrated that Al(III)- and Fe(II)-containing minerals can inhibit the growth of bacteria (McMahon et al., 2016). For Al(III)-containing minerals, their toxicity mainly depends on the release of Al(III), an extensively toxic element to bacteria (McMahon et al., 2016). However, Fe(II)-containing minerals usually cause oxidative damage to bacteria, i.e., the oxidative role of reactive oxygen species (ROS), particularly by involving hydroxyl radicals ($HO^{\bullet}$) that are generated by an Fe(II) catalyzed Fenton reaction where Fe(II) reacts with hydrogen peroxide (H_2O_2) to form $HO^{\bullet}$ radicals (Stohs and Bagchi, 1995; Williams et al., 2011; Wang et al., 2017a; Usman et al., 2018). However, it is unclear whether the common Fe(III)-containing minerals in soil have a similar inhibition

Biogeosciences Discuss., https://doi.org/10.5194/bg-2018-479
Manuscript under review for journal Biogeosciences
Discussion started: 10 December 2018

activity with Al(III)- and Fe(II)-containing minerals.

Taxonomically and ecologically diverse bacteria from terrestrial environments are a vast source of superoxide ($O_2^{\bullet-}$) and H_2O_2 (Diaz et al., 2013; Tang et al., 2013). Meanwhile, Fe(III)-containing minerals can catalyze the decomposition of H_2O_2 to generate strong oxidizing ROS (predominantly $HO^{\bullet}$ radical) through Fenton-like oxidation (equations 1-2) (Petigara et al., 2002; Garrido-Ramírez et al., 2010; Georgiou et al., 2015; Usman et al., 2016).

$$\equiv \text{Fe(III)-OH} + H_2O_2 \rightarrow \equiv \text{Fe(II)} + H_2O + HO_2^{\bullet} \quad (1)$$

$$\equiv \text{Fe(II)} + H_2O_2 \rightarrow \equiv \text{Fe(III)-OH} + HO^{\bullet} \quad (2)$$

where $\equiv \text{Fe(III)} - \text{OH}$ represents the iron mineral surface.

These Fenton-like reactions are well known as a type of heterogeneous catalysis (involving Fe minerals), which is distinct from homogeneous Fenton reactions (based on soluble Fe(II) in acidic media) (Garrido-Ramírez et al., 2010). The major advantage of heterogeneous catalysis is that it operates well over a wide range of pH values, while homogeneous catalysis displays optimal performance only at a pH of ~3 (Garrido-Ramírez et al., 2010). Furthermore, some researchers had demonstrated that surface Fe(II) was generated in the systems of H_2O_2 and ferric minerals (Kwan and Voelker, 2003; Polerecky et al., 2012). To date, the impact of Fe(III)-containing minerals on bacteria remains largely unexplored.

Here, we hypothesize that Fe(III)-containing minerals can inhibit the growth of bacteria through a free-radical mechanism (i.e., Fenton-like reactions). To test our hypothesis, we designed a series of cultivation experiments to monitor the growth of

Biogeosciences Discuss., https://doi.org/10.5194/bg-2018-479
Manuscript under review for journal Biogeosciences
Discussion started: 10 December 2018

Pseudomonas brassicacearum J12 in the presence of various minerals and in a mineral-free control. Various minerals, including montmorillonite, kaolinite, hematite, goethite and ferrihydrite, were used as the model Al(III)- or Fe(III)-containing minerals because they are broad-based in a wide range of soils (Cornell and Schwertmann, 2003; Meunier, 2005; Chesworth, 2008). Meanwhile, *Pseudomonas brassicacearum* J12 was selected as the model bacterium because it represents a major group of rhizobacteria that aggressively colonize plant roots in soils (Zhou et al., 2012). In this study, the objectives were to 1) examine and compare the bacterial inhibition properties of Al and Fe minerals; 2) build the correlation between solution chemistry and $HO^{\bullet}$ and the growth of bacteria; and 3) identify the mechanism by which Fe(III)-containing minerals inhibit bacteria. Throughout our experiments, the $HO^{\bullet}$ was trapped by terephthalic acid (TPA) (non-fluorescent), and the reaction's fluorescent product, i.e., 2-hydroxylterephthalic acid (HTPA) (Li et al., 2004), was quantitated in a high-performance liquid chromatography (HPLC) system. Correlative micro X-ray fluorescence (μ-XRF) and synchrotron-based Fourier transform infrared (SR-FTIR) spectroscopies were used to probe the *in situ* distribution and species of the Fe and extracellular polymeric substances (EPS), respectively (Luo et al., 2014; Sun et al., 2017a). X-ray photoelectron spectroscopy (XPS) was also used for analyzing the oxidation state(s) and speciation of Fe (Wilke et al., 2001; Yamashita and Hayes, 2008).

2. Materials and Methods

2.1. Cultivation experiments

Five minerals were selected in this study, including kaolinite (98%, Aladdin Reagent

Company, Shanghai, China), montmorillonite (98%, Aladdin Reagent Company, Shanghai, China) and synthetic hematite, goethite and ferrihydrite. All of the three iron minerals were synthesized by a previously described method (Schwertmann and Cornell, 2007). In brief, ferrihydrite was prepared by dissolving 40 g $Fe(NO_3)_3$•$9H_2O$ in 500 mL deionized water, and then 330 mL of 1 M KOH was added. Goethite was prepared by mixing 180 mL of 5 M KOH with 100 mL of 1 M $Fe(NO_3)_3$•$9H_2O$, and then the resulting mixture was aged for 60 h at 70 °C. Hematite was synthesized by mixing 2 L of 0.002 M HNO_3 (98 °C) with 16.16 g of $Fe(NO_3)_3$•$9H_2O$ and then aging for 7 d at 98 °C. Once prepared, all three suspensions were dialyzed with deionized water for 3 d to remove impurity ions, and then the pellets were air-dried. Powder X-ray diffraction (XRD) and FTIR analysis results for the used minerals are shown in Figs. S1-S2. All minerals were crushed and sieved through a 0.149 mm screen.

The bacterium used in this experiment is *Pseudomonas brassicacearum* J12, which is a major group of rhizobacteria that aggressively colonize plant roots, has been considered an important group for sustainable agriculture, and was provided by Dr. Zhou (Zhou et al., 2012). The stock strain of J12 was inoculated in Nutrient Broth (NB) medium to an optical density (OD_{600}) of ~0.6. The NB medium includes beef extract, 3 g L^{-1}; Tryptone, 5 g L^{-1}; yeast extract, 0.5 g L^{-1}; Glucose, 10 g L^{-1}. The cultivation system contained 9.5 mL of NB medium and 0.5 mL of J12, with a concentration of minerals of 5, 10 or 25 mg mL^{-1}. The final pH of the cultivation system was adjusted to 7.2. Next, the cultivation media were incubated for 12 h on a shaking incubator (180 rpm) at 28 °C. Then, 50 μL of the cultures were transferred to

Biogeosciences Discuss., https://doi.org/10.5194/bg-2018-479
Manuscript under review for journal Biogeosciences
Discussion started: 10 December 2018

fresh medium (10 mL) so that the effects of minerals were negligible. After 8 h growth, bacterial growth was monitored by measuring OD_{600} of the new culture and the photographs are shown as Fig. S3. The control experiment was performed without any mineral. All experiments were performed in triplicate. The particle size distribution of the applied raw minerals and the minerals after 12 h of incubation is listed in Table S1.

2.2. HPLC analysis

The $HO^{\bullet}$ was quantified in an Agilent 1260 Infinity HPLC system (Agilent Technologies, Inc., Germany) equipped with a Fluorescence Detector (G1321B) and a reverse-phase C18 column (Develosil ODS-UG5, 4.6 mm × 250 mm, Nomura Chemical Co., Japan). The mobile phase consisted of 200 mM K_2HPO_4 containing 2% of KCl (pH 4.37) and acetonitrile (90 : 10). Standard additions of 0, 0.05, 0.1, 0.5, and 1.0 µM HTPA were used to calibrate the HTPA response in each sample, with a linear response observed for all samples (Fig. S4). All experiments were performed in triplicate.

2.3. Correlative µ-XRF and SR-FTIR analysis

After 12 h growth, the original culture of the 25 mg mL^{-1} ferrihydrite treatment was frozen at −20 °C and directly sectioned without embedding. Then, thin sections (4 µm in thickness) were cut on a cryomicrotome (Cyrotome E, Thermo Shandon Limited, UK) and transferred to infrared-reflecting MirrIR Low-E microscope slides (Kevley Technologies, Ohio, USA).

Biogeosciences Discuss., https://doi.org/10.5194/bg-2018-479
Manuscript under review for journal Biogeosciences
Discussion started: 10 December 2018

The SR-FTIR analysis was obtained at beam-line BL01B1 of the National Center for Protein Science Shanghai (NCPSS). Spectra were recorded in reflectance mode using a Thermo Nicolet 6700 FTIR spectrometer and a continuum infrared microscope with the following settings: aperture size 15 μm, step size 10 × 10 μm^2, resolution 4 cm^{-1}, and 64 scans. Spectral maps were processed using Omnic 9.0 (Thermo Fisher Scientific Inc.). After baseline correction, map profiles of Fe-OH, C-H, C=O, C-N, and C-OH were created for peak heights at 3344, 2921, 1632, 1513, and 1030 cm^{-1}, respectively (Sun et al., 2017a and 2017b).

After SR-FTIR analysis, Fe image was collected at beamline 15U1 of Shanghai Synchrotron Radiation Facility (SSRF) for the same region of the thin section. Fluorescence maps (μ-XRF) of Fe were obtained by scanning the samples under a monochromatic beam at E = 10 keV with a step size of 2.3 × 3.3 μm^2 and a dwell time of 1 s. Then, two positions were selected for Fe K-edge μ-X-ray absorption near-edge structure (μ-XANES) analysis, and μ-XANES spectra were recorded using a 0.1 eV step size with a Si drift detector. Standard samples of hematite, goethite, ferrihydrite, iron(II) oxalate, and iron(III) oxalate were recorded in transmission mode. Iron(II) oxalate and iron(III) oxalate represent organic complexing ferrous and ferric, respectively, whereas hematite, goethite and ferrihydrite were used as the main iron mineral species. Linear combination fitting of standards was also performed for the μ-XANES spectra of samples, using ATHENA software (version 2.1.1). A standard was considered to have a substantial contribution if it accounted for more than 10% of a linear combination fit.

Biogeosciences Discuss., https://doi.org/10.5194/bg-2018-479
Manuscript under review for journal Biogeosciences
Discussion started: 10 December 2018

2.4. XPS analysis

The species of iron oxides were analyzed by XPS (PHI5000 Versa Probe, ULVAC-PHI, Japan). All the samples were freeze-dried and ground to fine powders prior to the XPS measurement. The XPS spectra were obtained with a monochromatized Al *K*α X-ray source (1486.6 eV) and the pressure in the analytical chamber was below 6×10^{-8} Pa (Yangzhou University). For wide scan spectra, an energy range of 0–1100 eV was used with the pass energy of 80 eV and the step size of 1 eV. The high-resolution scans were conducted according to the peak being examined with the pass energy of 40 eV and the step size of 0.06 eV. The precision of XPS was 0.06 eV. In order to obtain the oxidation status of surface sites, narrow scan spectra for Fe $2p_{3/2}$ were acquired. The carbon 1s electron binding energy corresponding to graphitic carbon at 284.8 eV was used as a reference for calibration purposes. Narrow scan spectra for Fe $2p_{3/2}$ were collected in binding energy forms and fitted using a least-squares curve-fitting program (XPSPEAK41 software). The XPS spectra were analyzed after subtracting the Shirley background that was applied for transition metals. The full width at half-maximum of those spectra was fixed constant between 1 and 3 and the percentage of Lorentzian–Gaussian was set at 20% for all the spectra.

2.5. Electron paramagnetic resonance (EPR) spectroscopy

The EPR spectra were recorded with a Bruker A300 X-band spectrometer (Guangxi University), which used a Gunn diode as microwave source and incorporated a

Biogeosciences Discuss., https://doi.org/10.5194/bg-2018-479
Manuscript under review for journal Biogeosciences
Discussion started: 10 December 2018

high-sensitivity cavity. Individual spectra were recorded over scan ranges of 500 and 30 mT to observe the signals originating from transition metal ions and free radicals, respectively. Details of additional spectra and all other acquisition parameters are given in the references (Goodman et al., 2016). The *g* values were calculated by reference to the Bruker ER4119HS-2100 marker accessory which has a *g* value of 1.9800. Spectral data were processed using the Bruker WinEPR software; with samples recorded with the same values for the microwave power, modulation amplitude, time constant and conversion time, intensities were determined both from double integration of complete spectra after background correction, and the heights of individual peaks, and corrected for any differences in the receiver gain or number of scans. Simulations of spectra to test the validity of various models for the C-centre spectrum were performed using the Bruker SimFonia software.

2.6. Chemical analysis

At cultivation time of 2 h and 12 h of the original cultures, portions of the samples were centrifuged at 16,000 *g* for 5 min, then filtered through a 0.45 µm membrane filter and analyzed with Inductively Coupled Plasma-Atomic Emission Spectroscopy (710/715 ICP-AES, Agilent, Australia) to detect the concentration of soluble Fe and Al. Total Fe and Fe(II) were determined with a modified 1,10-phenanthroline method (Amonette, 1998). Turbidity at 600 nm (a standard proxy for bacterial cell density) was measured using a Microplate Reader (Hach DR/2010) in mid-exponential phase. All experiments were performed in triplicate.

Biogeosciences Discuss., https://doi.org/10.5194/bg-2018-479
Manuscript under review for journal Biogeosciences
Discussion started: 10 December 2018

2.7. Statistical analysis

Significance was determined using one-way ANOVA followed by Tukey's HSD post hoc test, where the conditions of normality and homogeneity of variance were met; means ± SE (n = 3) that are followed by different letters indicate significant differences between treatments at $p < 0.05$. Microsoft Excel (2010), Origin Pro8 and SPSS (18.0) were used for drawing the graphs and data analysis.

3. Results

3.1. Bacterial inhibition by minerals

The effects of the nature and content of tested minerals on the OD_{600} of *Pseudomonas brassicacearum* J12 subcultures taken after 12 h growth are shown in Fig. 1. Compared to Control (i.e., no minerals), the presence of montmorillonite significantly increased OD_{600}. On the other hand, presence of all other investigated minerals decreased OD_{600} in the following order: ferrihydrite > goethite > hematite > kaolinite at 5 and 25 mg mL^{-1}, and ferrihydrite > goethite > kaolinite > hematite at 10 mg mL^{-1}, suggesting that montmorillonite promoted the growth of *Pseudomonas brassicacearum* J12, but the rest of the tested minerals inhibited its growth. Meanwhile, an increase in mineral concentration resulted in a significant decrease in OD_{600}, except for montmorillonite, as the OD_{600} seemed to be independent of its concentration (Fig. 1).

To further explore the factors influencing the bacterial growth by montmorillonite, electron paramagnetic resonance (EPR) spectra were used. The EPR spectra revealed that both the kaolinite and montmorillonite samples were dominated

by signals from structural Fe(III), which were located around 1600 gauss (g ~ 4.3) (Fig. 2). Iron oxides, which are commonly associated with these minerals produce a broad signal centred on ~ 3500 gauss (g ~ 2.0). However, the relatively weak resonance indicated that neither sample had appreciable amounts of iron oxides associated with it. The montmorillonite also showed a signal from Mn(II) and a free radical, whereas the free radical signal in the kaolinite was very weak, and there was no evidence of any Mn(II) signal in this sample. The Mn(II) in the montmorillonite was reported to act as a scavenger for any hydroxyl radical production (Garrido-Ramírez et al., 2010), which may explain the promotion of microbial growth.

3.2. Generation of $HO^{\bullet}$

A 12 h cultivation of *Pseudomonas brassicacearum* J12 in the presence of different minerals revealed that generation of $HO^{\bullet}$ radicals in the cases of montmorillonite, kaolinite and hematite was almost similar to the control (Fig. 3). However, presence of goethite and ferrihydrite significantly increased the production of $HO^{\bullet}$ radicals, which increased with an increase in their concentration. Specifically, in ferrihydrite treatments, the concentration of $HO^{\bullet}$ was approximately 260 nM at 5 and 10 mg mL^{-1} but increased rapidly to 450 nM at 25 mg mL^{-1}. In addition, the generation of $HO^{\bullet}$ at early growth (i.e., 2 h) was only detected with ferrihydrite at both 10 and 25 mg mL^{-1} and with goethite at 25 mg mL^{-1} (Fig. S5).

3.3. Iron chemistry and its correlation with $HO^{\bullet}$ and OD_{600}

To explore the factors affecting the generation of $HO^{\bullet}$ and the inhibition of *Pseudomonas brassicacearum* J12, we examined iron chemistry and its correlation

Biogeosciences Discuss., https://doi.org/10.5194/bg-2018-479
Manuscript under review for journal Biogeosciences
Discussion started: 10 December 2018

with $HO^{\bullet}$ and OD_{600} (Fig. 4). Much more soluble Fe was released from Fe(III)-containing minerals than from montmorillonite, kaolinite, and control (Fig. 4a). Additionally, a significant increase of soluble Fe was observed with the increase of ferrihydrite concentration. The solubility of Fe is closely related to pH value. Therefore, the solution pH was determined after 12 h growth of *Pseudomonas brassicacearum* J12 with different minerals and with no minerals (control) (Fig. S6). The range of solution pH varied from 4 to 6 for all of the treatments, expect for ferrihydrite treatment with a pH near 7. The pH decline suggests the production of organic acids by *Pseudomonas brassicacearum* J12. Thus, a high pH value in ferrihydrite treatment also support the inhibition of *Pseudomonas brassicacearum* J12. For all of the examined minerals, the trends of total Fe and Fe(II) were similar in the following order: ferrihydrite >> goethite > hematite > montmorillonite ≈ kaolinite ≈ control (Fig. 4b-4c).

Furthermore, a positive correlation exists between OD_{600} and soluble Fe content (R = 0.92, t = -3.49, p = 0.003) and Fe(II) (R = 0.98, t = -4.28, p =0.001) (Fig. 4d and 4f, Table S2). However, a significant but negative correlation between OD_{600} and soluble Fe (R = -0.75, t = 2.99, p = 0.009), and Fe(II) (R = -0.81, t = 2.27, p = 0.038) was found (Fig. 4g and 4i). Moreover, the correlation between $HO^{\bullet}$ and Fe(III) (R = 0.94, t = 1.38, p = 0.19), and between OD_{600} and Fe(III) (R = -0.80, t = 1.67, p = 0.116) were not significant (Fig. 4e and 4h). These results suggest that soluble Fe or Fe(II) may dominates the generation of $HO^{\bullet}$ and ultimately the inhibition of *Pseudomonas brassicacearum* J12. To test whether the release of Fe(III) to solution inhibit the growth of *Pseudomonas brassicacearum* J12 via a free-radical mechanism, we replaced Fe(III)-containing minerals by adding a series of concentrations of $Fe(NO_3)_3$, i.e., 0, 50 and 100 mg L^{-1}, in the cultivation experiments with the final pH of 7.2. The

Biogeosciences Discuss., https://doi.org/10.5194/bg-2018-479
Manuscript under review for journal Biogeosciences
Discussion started: 10 December 2018

results showed that addition of Fe(III) can inhibit the growth of *Pseudomonas brassicacearum* J12 (25-50%) by producing an additional $HO^{\bullet}$ concentration of 15 nM (Fig. S7), supporting the role of Fe(III) ion from solution in the initialization of a free-radical reaction.

290 In addition, we also examined soluble Al during the cultivation experiments (Fig. S8a) and found a high concentration of Al in the montmorillonite and kaolinite solutions. However, a weak correlation was found between soluble Al and $HO^{\bullet}$ (R = -0.35, t = -3.36, p = 0.004) and OD_{600} (R = 0.30, t = 2.24, p = 0.041) (Fig. S8b-8c), suggesting that the generation of $HO^{\bullet}$ and the inhibition of *Pseudomonas* 295 *brassicacearum* J12 is not contributed by Al.

3.4. In situ observation of Fe species and the distribution of organic functional groups

To explore the critical role of Fe chemistry in the inhibition of the growth of *Pseudomonas brassicacearum* J12, we used correlative μ-XRF and SR-FTIR 300 analyses for *in situ* measurement of the distribution of Fe species and EPS on the surface of ferrihydrite. The μ-XRF spectromicroscopy showed a distinct density of Fe distributed on iron particles (Fig. 5a). Two positions were selected for identifying the coordination state and species of Fe by μ-XANES spectra. Using hematite, goethite, ferrihydrite, iron(II) oxalate, and iron(III) oxalate as reference compounds, 305 the linear combination fitting (LCF) results from Fe K-edge μ-XANES spectra indicated that ferrihydrite was dominant (~82%), with a lesser percentage (~17%) of FeC_2O_4 among the mineral particles (Spot B in Fig. 5b and Table S3). However, considerable percentages of hematite (~13%) and goethite (~19%) were present on the edge of these mineral particles (Spot A in Fig. 5b and Table S3).

Biogeosciences Discuss., https://doi.org/10.5194/bg-2018-479
Manuscript under review for journal Biogeosciences
Discussion started: 10 December 2018

Furthermore, XPS analysis was conducted to investigate the oxidation state spectra for Fe 2p peak of samples (Fig. 6). The shift of the Fe $2p_{3/2}$ peak of 0.5 eV was observed between raw ferrihydrite and ferrihydrite after 12 h of cultivation with bacteria (Fig. 6a), suggesting the presence of reducing iron. Four Fe $2p_{3/2}$ peaks at 709.5 eV, 710.3 eV, 711.5 eV, 713.1 eV appeared in the F + bacteria treatment (Fig. 6b-6c). The peaks at 710.3 eV, 711.5 eV and 713.1 eV are regarded as multiplet peaks of Fe(III), but the peak at 709.5 eV is interpreted as Fe(II) (Grosvenor et al., 2004). Interestingly, the area of the peak at 709.5 eV was bigger in the F + bacteria treatment than that in F - bacteria treatment (Fig. 6b-6c), suggesting that Fe(II) was generated on the surface of ferrihydrite during the cultivation with bacteria. Based on the reaction 1, $HO_2^{\bullet}$ should be the oxidant products.

Furthermore, the SR-FTIR spectromicroscopy (Fig. 5c) showed that ferrihydrite (Fe-OH, 3344 cm^{-1}) had a similar distribution pattern with lipid (C-H, 2921 cm^{-1}), amide I (C=O, 1632 cm^{-1}), and amide II (C-N, 1513 cm^{-1}). However, polysaccharides (C-OH, 1030 cm^{-1}) seemed to be distributed only in the big mineral particles. Furthermore, correlation analysis confirmed good ($R \geq 0.68$, $p < 0.003$) linear correlations between ferrihydrite and these EPS (i.e., lipid, amide I, amide II, and polysaccharides) (Fig. S9), suggesting a close contact between ferrihydrite and the EPS components from *Pseudomonas brassicacearum* J12.

4. Discussion

4.1. Effect of Al(III)-containing minerals on the inhibition of bacterial growth

Our results showed that kaolinite (1 : 1 layer-type) resulted in significant inhibition of bacterial growth, but montmorillonite (2 : 1 layer-type) remarkably accelerated the

bacterial growth (Fig. 1). Similarly, recent studies have shown the toxic effects of aluminosilicate on microorganisms (Liu et al., 2016; Wilson and Butterfield, 2014), but the bacterial activity was not inhibited by the interfacial interactions between montmorillonite and bacteria (Wilson and Butterfield, 2014). It should be noted that the presence of minerals may potentially interfere with the measurement of cell numbers in Fig. 1. In this study, we subsampled the experimental cultures and diluted them in fresh medium so that both clay particles and bacteria were 200× less concentrated (Fig. S3), following the protocol of McMahon et al. (2016). As a result, the effect of mineral concentration may be minimal. In addition, plating the bacteria by evaluating populations by counting colonies may act as a complementary method for OD_{600} and needs to be investigated in the future.

It is generally accepted that diverse bacteria are susceptible to Al(III). A previous study showed that a 58 μM (~1.6 mg L^{-1}) concentration of Al has toxicological effects on *Pseudomonas sp.* (Illmer and Schinner, 1999). In the present study, the amount of aqueous Al(III) exceeded 2 mg L^{-1} for all kaolinite experiments while its concentration was negligible in the presence of montmorillonite during the early growth of bacteria (Fig. S8). Thus, the inhibition of bacterial activity by kaolinite may possibly be attributed to the toxicity of aqueous Al(III). Specifically, Al(III) reacts with membrane phospholipids and then increases membrane permeability that leads to the inactivation of bacteria (Londono et al., 2017).

In addition, some essential elements (e.g., Mg and P) can be affected by Al(III) for bacterial absorption, which could also limit bacterial growth (Piña and Cervantes, 1996; Londono et al., 2017). Furthermore, the formation of some Al intermediates by the decreasing pH, such as $Al_{13}O_4(OH)_{24}^{7+}$, is also suggested to be more toxic for

bacterial growth (Amonette et al., 2003; Liu et al., 2016). It is worth noting that >2 mg L^{-1} of aqueous Al(III) was detected for montmorillonite experiments with the passage of time (Fig. S8); however, the bacterial growth was not inhibited (Fig. 1). This may be attributed to the adsorption of aqueous Al(III) by bacterial EPS, which further protected bacteria from damage (Wu et al., 2014). However, direct evidence is lacked in this study and thus further investigation is needed to address this issue.

4.2. Inhibition of bacteria by Fe(III)-containing minerals via a free-radical mechanism

Our results showed that Fe(III)-containing minerals resulted in higher generation of $HO^{\bullet}$ and had higher bacterial inhibition efficiency than Al(III)-containing minerals (Figs. 1 and 3). Fe is widely known as a transition metal that might cause microbial inactivation through ROS-mediated cellular damage, i.e., genotoxicity, protein dysfunction and impaired membrane function (Lemire et al., 2013). Inhibition of bacteria by Fe minerals is generally attributed to the generation of $HO^{\bullet}$ through a Fenton reaction (Morrison et al., 2016) or Fenton-like reaction (Garrido-Ramírez et al., 2010). Due to its amorphous structure, high reactive surface area and solubility, ferrihydrite (~200-300 m^2 g^{-1}) is more likely to physically interact with bacterial surfaces than hematite (~30 m^2 g^{-1}) and goethite (~20 m^2 g^{-1}) (Schwertmann and Cornell, 2007; Lemire et al., 2013). A recent study demonstrated that metal oxide nanoparticles produced more ROS than bulk metal oxides (Wang et al., 2017a). In this study, we observed higher $HO^{\bullet}$ formation and stronger inhibition of bacteria in ferrihydrite treatments (Figs. 1 and 3), suggesting that reactive surface area and solubility has a significant effect on enhancing formation of $HO^{\bullet}$ and bacterial inhibition activity. Reactive mineral surfaces can catalyze $HO^{\bullet}$ generation or act as

Biogeosciences Discuss., https://doi.org/10.5194/bg-2018-479
Manuscript under review for journal Biogeosciences
Discussion started: 10 December 2018

"carriers" where $HO^{\bullet}$-inducing materials are adsorbed (Schoonen et al., 2006). In our experiment, there was a lesser amount of $HO^{\bullet}$ produced with the different concentrations of aqueous $Fe(NO_3)_3$ (Fig. S7) than with the iron minerals (Fig. 3). In line with other studies (Kwan and Voelker, 2003; Wang et al., 2017b), we deduced that $HO^{\bullet}$ may mainly generate on the mineral surface, partly due to the positive charge of mineral surface (Tombácz and Szekeres, 2006) but the negative charge of microbes (Jucket et al., 1996).

A recent study demonstrated that surface rather than aqueous Fe(II) plays a dominant role in producing extracellular $HO^{\bullet}$ that damage cell membrane lipid revealed by in-situ imaging (Wang et al., 2017b). The following reactions (equations 3-4) reveal that the generation of $HO^{\bullet}$ is catalyzed by surface Fe(II) (Kwan and Voelker, 2003; Polerecky et al., 2012):

$$\equiv Fe(III) + H_2O_2 \rightarrow \equiv Fe(II) + H^+ + HO_2^{\bullet} \quad (3)$$

$$\equiv Fe(II) + H_2O_2 \rightarrow \equiv Fe(III) + HO^{\bullet} + OH^- \quad (4)$$

In this study, a substantial amount of Fe(II) was generated by ferrihydrite, approximately 4-fold higher than soluble Fe (Fig. 4). This amount of Fe(II) included two portions: one existed in solution, another was derived from the mineral surface. To further confirm the generation of surface Fe(II), Fe K-edge μ-XANES analysis were used, and they showed that ferrihydrite presented various Fe species, and Fe(II) increased from 17.3% among the mineral particles (A position) to 25.9% in the edge of mineral particles (B position) (Fig. 5 and Table S3). High percentage of the less stable ferrihydrite (Table S3) may be attributable to the stabilization role of produced EPS (Fig. 5c) by bacteria to minerals, which had been shown during the cultivation of

Biogeosciences Discuss., https://doi.org/10.5194/bg-2018-479
Manuscript under review for journal Biogeosciences
Discussion started: 10 December 2018

fungi with minerals (Li et al., 2016). Note that the LCF results are dependent on the range of compounds used to generate the reference spectrum library, which is one drawback of LCF. To further support the LCF results, XPS being a near-surface sensitive technique is also used to detect the production of ferrous iron at the surface of the iron oxides, owing to a greater certainty than LCF and XANES to demonstrate the presence of ferrous iron by fitting multiplet-splitting models (Grosvenor et al., 2004). According to the XPS analysis, the Fe $2p_{3/2}$ peak shifted from high energy (F – bacteria) to low energy (F + bacteria) (Fig. 6), revealing that Fe(II) was produced on the surface of ferrihydrite during cultivation.

In addition to Fenton-like reactions (Garrido-Ramírez et al., 2010), Fe(II) can also be generated by catalyzing a series of cellular intracellular (e.g., glutathione and NAD(P)H) and free (e.g., L-cysteine and $FADH_2$) reductants (Imlay, 2003). Other metabolically formed oxidants released by bacteria may also contribute to Fe(II) oxidation (Melton et al., 2014). Subsequently, the oxidation of Fe(II) to Fe(III) is followed by a reduction of the Fe(III) to Fe(II) (Melton et al., 2014). In addition, many microorganisms are thought to transfer electrons between their cytoplasmic membranes and extracellular minerals through a network of redox and structural c-type cytochromes (c-Cyts) and flavins (Shi et al., 2016). The redox cycling of Fe during interfacial interactions between Fe(III)-containing minerals and bacteria accelerates the generation of $HO^{\bullet}$ (Page et al., 2013).

The responses of bacterial inhibition activity followed the order Fe(III)-containing minerals > $Fe(NO_3)_3$ > Control (Figs. 1 and S7). Intracellular oxidative toxicity caused by soluble Fe(III) played an important role in bacterial inhibition activity simultaneously (Schoonen et al., 2006). We deduced that inhibition of bacteria with

Biogeosciences Discuss., https://doi.org/10.5194/bg-2018-479
Manuscript under review for journal Biogeosciences
Discussion started: 10 December 2018

Fe(III)-containing minerals mainly depends on the coupled effect of soluble Fe, surface Fe(II), and extracellular $HO^{\bullet}$.

4.3. Inhibition of bacterial growth by a free-radical mechanism and its implications for soil carbon storage

In this study, we proposed a schematic of Fe(III)-containing minerals inhibiting bacterial growth through a free-radical mechanism (Fig. 7). Surface Fe(II) is produced from the reduction of Fe(III) on the surface of Fe(III)-containing minerals, promoting the production of $HO^{\bullet}$ through the Fenton or Fenton-like reactions (Garrido-Ramírez et al., 2010). Oxidative damage of extracellular $HO^{\bullet}$ may lead to bacterial inactivation, and protection of carbon from microbial degradation. In addition, the generation of free radicals may also have indirect effects on bacterial growth via substrate availability (Table S4). Substrate availability is improved in the presence of radicals, owing to the following two facts: 1) the depolymerization role of radicals on the complex substrates; 2) the inhibition role of radicals on bacteria indirectly increasing the amounts of available substrates.

Microbes affect the cycling of soil organic carbon (SOC), and their products are important components of SOC (Kögel-Knabner, 2002; Kleber and Johnson, 2010; Schmidt et al., 2011; Liang et al., 2017). In this study, we suggest that soil carbon storage is regulated by Fe minerals, not only because of the formation of organo-mineral complexes (Kögel-Knabner, 2002; Kleber and Johnson, 2010; Schmidt et al., 2011) but also due to the bacterial inhibition activity of Fe minerals. However, it should be noted that NB medium containing casein and meat hydrolysates is only a medium that enables the growth of *Pseudomonas brassicacearum* J12 in this study, but it is far away from organic matter decomposition or substrates available in

soil systems. Further investigation should be conducted to explore the effect of microbe-driven Fenton-like reaction on the storage of SOC in soil system in the future.

5. Conclusions

Kaolinite, hematite, goethite and ferrihydrite had a significant inhibitory effect on the growth of *Pseudomonas* J12, which was more prominent with a higher concentration, following the order 25 mg mL^{-1} > 10 mg mL^{-1} > 5 mg mL^{-1}. In contrast, montmorillonite promoted the growth of *Pseudomonas* J12, which was independent on its concentration. Compared to Al(III)-containing minerals, Fe(III)-containing minerals promoted more $HO^{\bullet}$ generation and thus increased suppression to *Pseudomonas* J12 via a free-radical mechanism. Furthermore, our results revealed that surface Fe(II) was produced on the mineral surface that may act as a catalyst, promoting the generation of $HO^{\bullet}$ rather than soluble Fe. The generation of $HO^{\bullet}$ by Fe(III)-containing minerals follows the order ferrihydrite > goethite > hematite. In addition, the generation of free radicals may also have indirect (i.e., substrate availability) effects on bacterial growth and the presence of minerals may potentially interfere with the measurement of cell numbers. In summary, our findings indicate that the inhibition of bacteria with Fe(III)-containing minerals mainly depends on the coupled effect of soluble Fe and extracellular $HO^{\bullet}$, which may further contribute to soil carbon storage.

The Supplement related to this article is available online at **http://www.biogeosciences.net/.**

Acknowledgments. We thank the staff for their support at BL01B beamline of National Center for Protein Sciences Shanghai (NCPSS) and BL15U1 at Shanghai Synchrotron Radiation Facility (SSRF), for assistance during data collection. This work was funded by the National Key Research and Development Program of China (2017YFD0800803) and the National Natural Science Foundation of China (41671294 and 41371248).

Biogeosciences Discuss., https://doi.org/10.5194/bg-2018-479
Manuscript under review for journal Biogeosciences
Discussion started: 10 December 2018

References

Amonette, J. E.: Improvements to the quantitative assay of nonrefractory minerals for Fe(II) and total Fe using 1,10-Phenanthroline, Clays Clay Miner., 46, 51-62, 1998.

Amonette, J. E., Russell, C. K., Carosino, K. A., Robinson, N. L., and Ho, J. T.: Toxicity of Al to desulfovibrio desulfuricans, Appl. Environ. Microbiol., 69, 4057-4066, 2003.

Bruun, T. B., Elberling, B., and Christensen, B. T.: Lability of soil organic carbon in tropical soils with different clay minerals, Soil Biol. Biochem., 42, 888-895, 2010.

Chesworth, W.: Encyclopedia of Soil Science, Springer, 2008.

Cornell, R. M., and Schwertmann, U.: The iron oxides: structure, properties, reactions, occurences and uses, Wiley-VCH Verlag GmbH & Co. KGaA, 2003.

Diaz, J. M., Hansel, C. M., Voelker, B. M., Mendes, C. M., Andeer, P. F., and Zhang, T.: Widespread production of extracellular superoxide by heterotrophic bacteria, Science, 340, 1223-1226, 2013.

Garrido-Ramírez, E. G., Theng, B. K. G., and Mora, M. L.: Clays and oxide minerals as catalysts and nanocatalysts in Fenton-like reactions - A review, Appl. Clay Sci., 47, 182-192, 2010.

Georgiou, C. D., Sun, H. J., McKay, C. P., Grintzalis, K., Papapostolou, I., Zisimopoulos, D., Panagiotidis, K., Zhang, G., Koutsopoulou, E., Christidis, G.E., and Margiolaki, I.: Evidence for photochemical production of reactive

oxygen species in desert soils, Nat. Commun., 6, 7100, 2015.

Goodman, B. A., Worasith, N., and Deng, W.: EPR spectra of a new radiation-induced paramagnetic centre in kaolins, Clay Miner., 51, 707-714, 2016.

Grosvenor, A. P., Kobe, B. A., Biesinger, M. C., and McIntyre, N. S.: Investigation of multiplet splitting of Fe 2p XPS spectra and bonding in iron compounds, Surf. Interface Anal., 36, 1564-1574, 2004.

Illmer, P., and Schinner, F.: Influence of nutrient solution on Al-tolerance of *Pseudomonas* sp., FEMS Microbiol. Lett., 170, 187-190, 1999.

Imlay, J. A.: Pathways of oxidative damage, A Annu. Rev. Microbiol., 57, 395-418, 2003.

Jucker, B. A., Harms, H., and Zehnder, A. J. B.: Adhesion of the positively charged bacterium *Stenotrophomonas (Xanthomonas) maltophilia* 70401 to glass and teflon, J. Bacteri., 178, 5472-5479, 1996.

Kleber, M., and Johnson, M. G.: Chapter 3 - Advances in Understanding the Molecular Structure of Soil Organic Matter: Implications for Interactions in the Environment. Advances in Agronomy, Donald, L.S. (ed), pp. 77-142, Academic Press, 2010.

Kögel-Knabner, I.: The macromolecular organic composition of plant and microbial residues as inputs to soil organic matter, Soil Biol. Biochem., 34, 139-162, 2017.

Kwan, W. P., and Voelker, B. M.: Rates of hydroxyl radical generation and organic

compound oxidation in mineral-catalyzed Fenton-like systems, Environ. Sci. Technol., 37, 1150-1158, 2003.

Lemire, J. A., Harrison, J. J., and Turner, R. J.: Antimicrobial activity of metals: mechanisms, molecular targets and applications. Nat. Rev. Microbiol., 11, 371-384, 2013.

Li, L., Abe, Y., Nagasawa, Y., Kudo, R., Usui, N., Imai, K., Mashino, T., Mochizuki, M., and Miyata, N.: An HPLC assay of hydroxyl radicals by the hydroxylation reaction of terephthalic acid, Biomed. Chromatogr., 18, 470-474, 2004.

Liang, C., Schimel, J. P., and Jastrow, J. D.: The importance of anabolism in microbial control over soil carbon storage, Nat. Microbiol., 2, 17105, 2017.

Liu, D., Dong, H., Agrawal, A., Singh, R., Zhang, J., and Wang, H.: Inhibitory effect of clay mineral on methanogenesis by *Methanosarcina mazei* and *Methanothermobacter* thermautotrophicus, Appl. Clay Sci., 126, 25-32, 2016.

Londono, S. C., Hartnett, H. E., and Williams, L. B.: Antibacterial activity of aluminum in clay from the Colombian Amazon, Environ. Sci. Technol., 51, 2401-2408, 2017.

Luo, L., Lv, J., Xu, C., and Zhang, S.: Strategy for characterization of distribution and associations of organobromine compounds in soil using synchrotron radiation based spectromicroscopies, Anal. Chem., 86, 11002-11005, 2014.

McMahon, S., Anderson, R. P., Saupe, E. E., and Briggs, D. E. G.: Experimental evidence that clay inhibits bacterial decomposers: Implications for preservation of organic fossils, Geology, 44, 867-870, 2016.

Melton, E. D., Swanner, E. D., Behrens, S., Schmidt, C., and Kappler, A.: The interplay of microbially mediated and abiotic reactions in the biogeochemical Fe cycle, Nat. Rev. Microbiol., 12, 797-808, 2014.

Meunier, A.: Clays, Springer Berlin Heidelberg, New York, 2005.

Morrison, K. D., Misra, R., and Williams, L. B.: Unearthing the antibacterial mechanism of medicinal clay: A geochemical approach to combating antibiotic resistance, Sci. Rep. 6, 19043, 2016.

Morrison, K. D., Underwood, J. C., Metge, D. W., Eberl, D. D., and Williams, L. B.: Mineralogical variables that control the antibacterial effectiveness of a natural clay deposit, Environ. Geochem. Hlth., 36, 613-631, 2013.

Page, S. E., Kling, G. W., Sander, M., Harrold, K. H., Logan, J. R., McNeill, K., and Cory, R. M.: Dark formation of hydroxyl radical in arctic soil and surface waters, Environ. Sci. Technol., 47, 12860-12867, 2013.

Petigara, B. R., Blough, N. V., and Mignerey, A. C.: Mechanisms of hydrogen peroxide decomposition in soils, Environ. Sci. Technol., 36, 639-645, 2002.

Piña, R. G., and Cervantes, C.: Microbial interactions with aluminium, Biometals, 9, 311-316, 1996.

Polerecky, L., Adam, B., Milucka, J., Musat, N., Vagner, T., and Kuypers, M.M.: Look@NanoSIMS--a tool for the analysis of nanoSIMS data in environmental microbiology, Environ. Microbiol., 14, 1009-1023, 2012.

Schmidt, M. W., Torn, M. S., Abiven, S., Dittmar, T., Guggenberger, G., Janssens, I. A., Kleber, M., Kogel-Knabner, I., Lehmann, J., Manning, D. A., Nannipieri, P.,

Rasse, D. P., Weiner, S., and Trumbore, S. E. Persistence of soil organic matter as an ecosystem property, Nature, 478, 49-56, 2011.

Schoonen, M. A. A., Cohn, C. A., Roemer, E., Laffers, R., Simon, S. R., and O'Riordan, T.: Mineral-induced formation of reactive oxygen species, Rev. Mineral. Geochem., 64, 179-221, 2006.

Schwertmann, U., and Cornell, R. M.: Iron Oxides in the Laboratory: Preparation and characterization, Schwertmann, U. and Cornell, R.M. (eds), pp. 121-134, Wiley-VCH Verlag GmbH, 2007.

Shi, L., Dong, H. L., Yu, H. Q., Reguera, G., Beyenal, H., Lu, A. H., and Fredrickson, J. K.: Extracellular electron transfer mechanisms between microorganisms and minerals, Nat. Rev. Microbiol., 14, 651-662, 2016.

Stohs, S. J., and Bagchi, D.: Oxidative mechanisms in the toxicity of metal-ions, Free Radical Bio. Med., 18, 321-336, 1995.

Sun, F. S., Li, Y. Q., Wang, X., Chi, Z. L., and Yu, G. H.: Using new hetero-spectral two-dimensional correlation analyses and synchrotron-radiation-based spectromicroscopy to characterize binding of Cu to soil dissolved organic matter, Environ. Pollut., 223, 457-465, 2017a.

Sun, F. S., Polizzotto, M. L., Guan, D. X., Wu, J., Shen, Q. R., Ran, W., Wang, B. R., and Yu, G. H.: Exploring the interactions and binding sites between Cd and functional groups in soil using two-dimensional correlation spectroscopy and synchrotron radiation based spectromicroscopies, J. Hazard. Mater., 326, 18-25, 2017b.

590 Tang, Y. Z., Zeiner, C. A., Santelli, C. M., and Hansel, C. M.: Fungal oxidative dissolution of the Mn(II)-bearing mineral rhodochrosite and the role of metabolites in manganese oxide formation, Environ. Microbiol., 15, 1063-1077, 2013.

Tombacz, E., and Szekeres, M.: Surface charge heterogeneity of kaolinite in aqueous
595 suspension in comparison with montmorillonite, Appl. Clay Sci., 34, 105-124. 2006.

Usman, M., Byrne, J. M., Chaudhary, A., Orsetti, S., Hanna, K., Ruby, C., Kappler, A., and Haderlein, S. B.: Magnetite and green rust: Synthesis, properties, and environmental applications of mixed-valent iron minerals. Chem. Rev., 118,
600 3251-3304, 2018.

Usman, M., Hanna, K., and Haderlein, S.: Fenton oxidation to remediate PAHs in contaminated soils: A critical review of major limitations and counter-strategies, Sci. Total Environ., 569-570, 179-190, 2016.

Wang, X., Dong, H., Zeng, Q., Xia, Q., Zhang, L., and Zhou, Z.: Reduced
605 iron-containing clay minerals as antibacterial agents, Environ. Sci. Technol., 51, 7639-7647, 2017a.

Wang, D., Zhao, L., Ma, H., Zhang, H., and Guo, L. H.: Quantitative analysis of reactive oxygen species photogenerated on metal oxide nanoparticles and their bacteria toxicity: The role of superoxide radicals, Environ. Sci. Technol., 51,
610 10137-10145, 2017b.

Wilke, M., Farges, F., Petit, P. E., Brown, G. E., and Martin, F.: Oxidation state and

coordination of Fe in minerals: An Fe *K*-XANES spectroscopic study, Am. Mineral., 286, 714-730, 2001.

Williams, L. B.: Geomimicry: Harnessing the antibacterial action of clays, Clay Miner., 52, 1-24, 2017.

Williams, L. B., and Haydel, S. E.: Evaluation of the medicinal use of clay minerals as antibacterial agents, Int. Geol. Rev., 52, 745-770, 2010.

Williams, L. B., Haydel, S. E., Jr, R. F. G., and Eberl, D. D.: Chemcial and mineralogical charcteristics of French green clays used for healing, Clays Clay Miner., 56, 437-452, 2008.

Williams, L. B., Metge, D. W., Eberl, D. D., Harvey, R. W., Turner, A. G., Prapaipong, P., and Poret-Peterson, A. T.: What makes a natural clay antibacterial? Environ. Sci. Technol., 45, 3768-3773, 2011.

Wilson, L. A., and Butterfield, N. J.: Sediment effects on the preservation of Burgess Shale-Type compression fossils, Palaios, 29, 145-154, 2014.

Wu, H., Chen, W., Rong, X., Cai, P., Dai, K., and Huang, Q.: Soil colloids and minerals modulate metabolic activity of measured using microcalorimetry, Geomicrobiol. J., 31, 590-596, 2014.

Yamashita, T., and Hayes, P.: Analysis of XPS spectra of Fe^{2+} and Fe^{3+} ions in oxide materials, Appl. Surf. Sci., 254, 2441-2449, 2008.

Yu, G. H., Xiao, J., Hu, S. J., Polizzotto, M. L., Zhao, F. J., McGrath, S. P., Li, H., Ran, W., and Shen, Q. R.: Mineral availability as a key regulator of soil carbon storage, Environ. Sci. Technol., 51, 4960-4969, 2017.

Zhou, T., Chen, D., Li, C., Sun, Q., Li, L., Liu, F., Shen, Q., and Shen, B.: Isolation and characterization of *Pseudomonas brassicacearum* J12 as an antagonist against ralstonia solanacearum and identification of its antimicrobial components, Microbiol. Res., 167, 388-394, 2012.

Biogeosciences Discuss., https://doi.org/10.5194/bg-2018-479
Manuscript under review for journal Biogeosciences
Discussion started: 10 December 2018

Figure Captions

Figure 1. Optical density at 600 nm (OD_{600}) of 8-h-old *Pseudomonas brassicacearum* J12 subcultures taken after 12 h growth with different minerals and with no minerals (control). K, kaolinite; M, montmorillonite; H, hematite; G, goethite; F, ferrihydrite; C, Control (i.e., no mineral). Values are the mean ± SE (n = 3).

Figure 2. Wide scan EPR spectra of both the kaolinite and montmorillonite.

Figure 3. Generation of hydroxyl radical ($HO^{\bullet}$) after 12 h growth of *Pseudomonas brassicacearum* J12 with different minerals and with no minerals (control). K, kaolinite; M, montmorillonite; H, hematite; G, goethite; F, ferrihydrite; C, Control (i.e., no mineral). Values are the mean ± SE (n = 3).

Figure 4. Iron chemistry (a-c) and its correlation with hydroxyl radical ($HO^{\bullet}$) (d-f) as well as optical density at 600 nm (OD_{600}) (g-i). (a) soluble Fe. (b) total Fe. (c) Fe(II). (d) soluble Fe vs $HO^{\bullet}$. (e) total Fe vs $HO^{\bullet}$. (f) Fe(II) vs $HO^{\bullet}$. (g) soluble Fe vs OD_{600}. (h) total Fe vs OD_{600}. (i) Fe(II) vs OD_{600}. K, kaolinite; M, montmorillonite; H, hematite; G, goethite; F, ferrihydrite; C, Control (i.e., no mineral). Values in (a-c) are the mean ± SE (n = 3).

Figure 5. Correlative micro X-ray fluorescence (μ-XRF) and synchrotron-based Fourier transform infrared (SR-FTIR) analysis of the thin section from the cultures of the 25 mg/mL ferrihydrite treatment after 12 h cultivation. (a) μ-XRF map. (b) The LCF fitting of μ-X-ray absorption near-edge structure (XANES) analysis the selected

regions of interest (ROI) region (i.e., A and B). (c) SR-FTIR maps. The color scale in (c) is a relative scale for each peak height and does not allow quantitative comparisons between peaks.

Figure 6. (a) Fe 2p X-ray photoelectron spectroscopy (XPS) spectra of ferrihydrite samples, F+bacteria and F-bacteria; (b-c) Fe 2p 3/2 spectra of F+bacteria and F-bacteria, respectively, during the cultivation (12 h). F+bacteria, ferrihydrite with bacteria; F-bacteria, ferrihydrite without bacteria.

Figure 7. Schematic of the bacterial inhibition by Fe(III)-containing minerals through a free-radical mechanism.

Biogeosciences Discuss., https://doi.org/10.5194/bg-2018-479
Manuscript under review for journal Biogeosciences
Discussion started: 10 December 2018

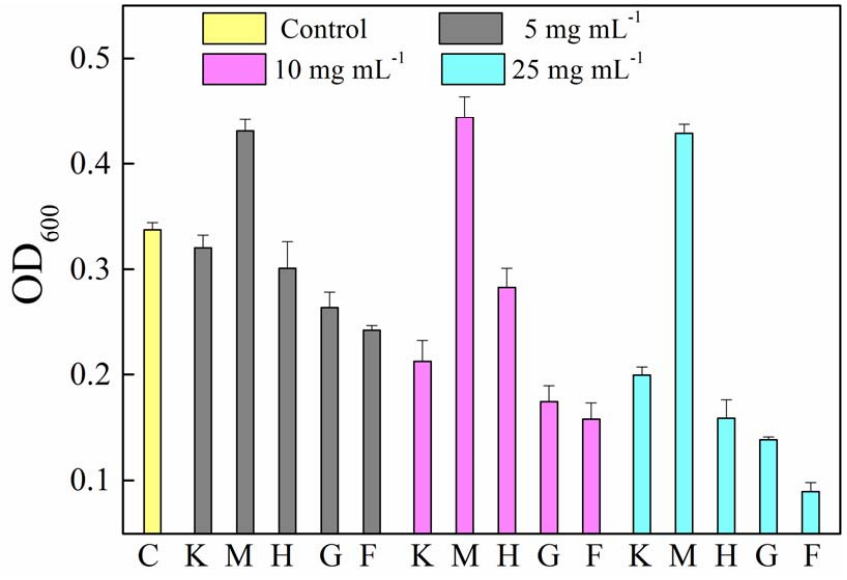

670 **Figure 1.** Optical density at 600 nm (OD_{600}) of 8-h-old *Pseudomonas brassicacearum* J12 subcultures taken after 12 h growth with different minerals and with no minerals (control). K, kaolinite; M, montmorillonite; H, hematite; G, goethite; F, ferrihydrite; C, Control (i.e., no mineral). Values are the mean ± SE (n = 3).

Biogeosciences Discuss., https://doi.org/10.5194/bg-2018-479
Manuscript under review for journal Biogeosciences
Discussion started: 10 December 2018

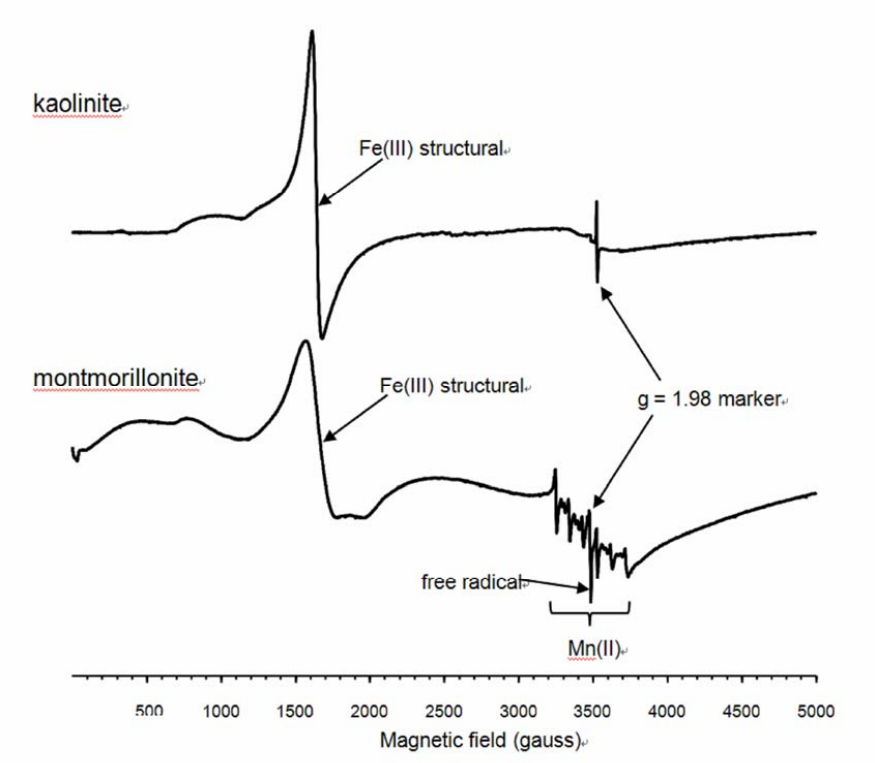

675 **Figure 2**. Wide scan EPR spectra of both the kaolinite and montmorillonite.

Biogeosciences Discuss., https://doi.org/10.5194/bg-2018-479
Manuscript under review for journal Biogeosciences
Discussion started: 10 December 2018

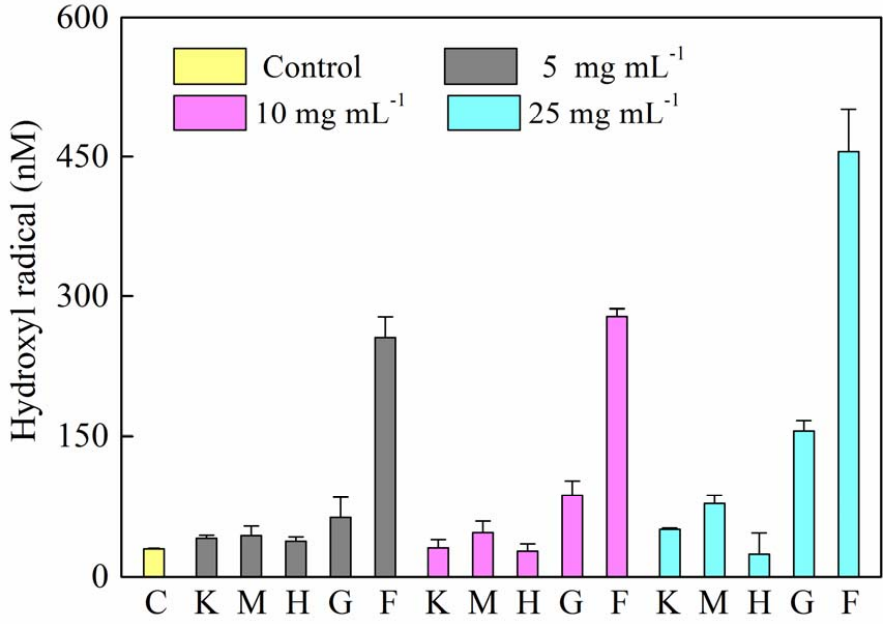

Figure 3. Generation of hydroxyl radical ($HO^{\bullet}$) after 12 h growth of *Pseudomonas brassicacearum* J12 with different minerals and with no minerals (control). K, kaolinite; M, montmorillonite; H, hematite; G, goethite; F, ferrihydrite; C, Control (i.e., no mineral). Values are the mean ± SE (n = 3).

Biogeosciences Discuss., https://doi.org/10.5194/bg-2018-479
Manuscript under review for journal Biogeosciences
Discussion started: 10 December 2018

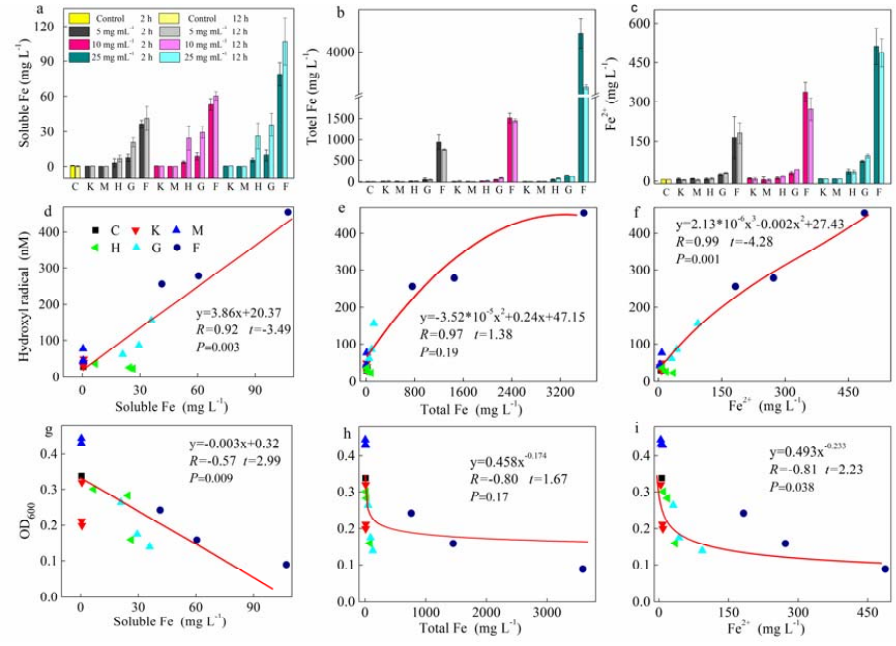

Figure 4. Iron chemistry (a-c) and its correlation with hydroxyl radical ($HO^{\bullet}$) (d-f) as well as optical density at 600 nm (OD_{600}) (g-i). (a) soluble Fe. (b) total Fe. (c) Fe(II). (d) soluble Fe vs $HO^{\bullet}$. (e) total Fe vs $HO^{\bullet}$. (f) Fe(II) vs $HO^{\bullet}$. (g) soluble Fe vs OD_{600}. (h) total Fe vs OD_{600}. (i) Fe(II) vs OD_{600}. K, kaolinite; M, montmorillonite; H, hematite; G, goethite; F, ferrihydrite; C, Control (i.e., no mineral). Values in (a-c) are the mean ± SE (n = 3).

Biogeosciences Discuss., https://doi.org/10.5194/bg-2018-479
Manuscript under review for journal Biogeosciences
Discussion started: 10 December 2018

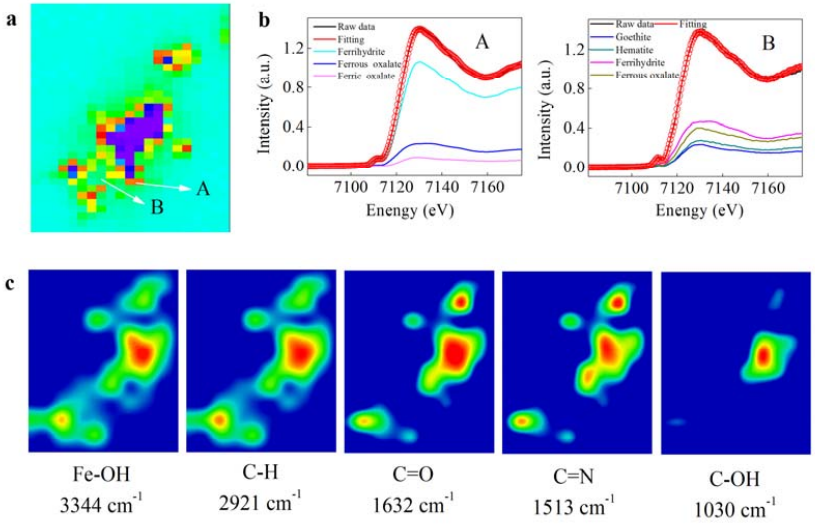

Figure 5. Correlative micro X-ray fluorescence (μ-XRF) and synchrotron-based Fourier transform infrared (SR-FTIR) analysis of the thin section from the cultures of the 25 mg/mL ferrihydrite treatment after 12 h cultivation. (a) μ-XRF map. (b) The LCF fitting of μ-X-ray absorption near-edge structure (XANES) analysis the selected regions of interest (ROI) region (i.e., A and B). (c) SR-FTIR maps. The color scale in (c) is a relative scale for each peak height and does not allow quantitative comparisons between peaks.

Biogeosciences Discuss., https://doi.org/10.5194/bg-2018-479
Manuscript under review for journal Biogeosciences
Discussion started: 10 December 2018

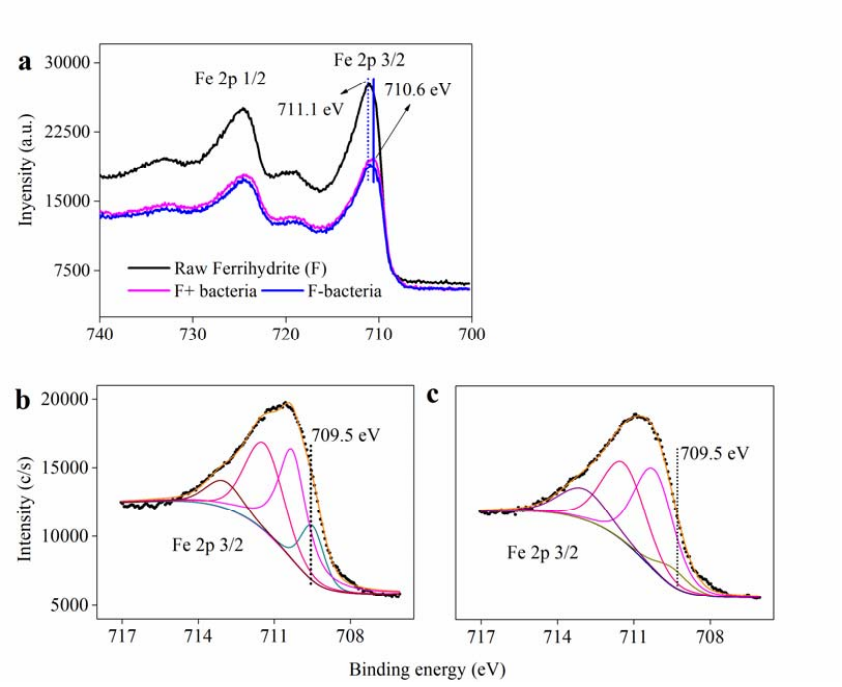

Figure 6. (a) Fe 2p X-ray photoelectron spectroscopy (XPS) spectra of ferrihydrite samples, F+bacteria and F-bacteria; (b-c) Fe 2p 3/2 spectra of F+bacteria and F-bacteria, respectively, during the cultivation (12 h). F+bacteria, ferrihydrite with bacteria; F-bacteria, ferrihydrite without bacteria.

Biogeosciences Discuss., https://doi.org/10.5194/bg-2018-479
Manuscript under review for journal Biogeosciences
Discussion started: 10 December 2018

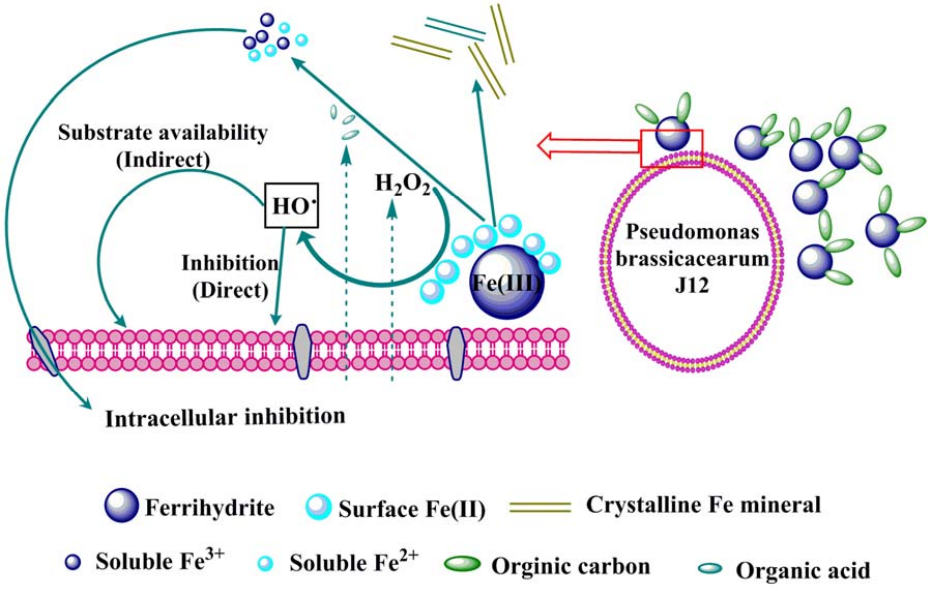

Figure 7. Schematic of the bacterial inhibition by Fe(III)-containing minerals through a free-radical mechanism.